Management Systems
in
Production Engineering

2025, Volume 33, Issue 3, pp. 380-387

Date of submission of the article to the Editor: 02/2025
Date of acceptance of the article by the Editor: 07/2025

DOI 10.2478/mspe-2025-0036

IMPROVING BALLISTIC RESISTANCE OF ARMOR STEEL BY FCAW WITH HARDFACING ALLOYS OF Fe–Mo–Mn–B–C SYSTEM

Pavlo Prysyazhnyuk
Ivano-Frankivsk National Technical University of Oil and Gas

Witold Biały
KOMAG Institute of Mining Technology

Michał Bembenek
AGH University of Krakow

Vitalii Panchuk, Iuliia Medvid
Ivano-Frankivsk National Technical University of Oil and Gas

Zoia Duriagina
Lviv Polytechnic National University

Taras Romanyshyn, Vasyl Vytvytskyi
Ivano-Frankivsk National Technical University of Oil and Gas

Abstract:
Armor steels can be strengthened against modern ballistic threats through surface hardfacing with advanced Fe-based alloys. This study develops a series of flux-cored arc welded (FCAW) hardfacing alloys in the Fe–Mo–Mn–B–C system to enhance the ballistic resistance of Armox® 440T steel. Single-layer (~3 mm) hardfacings were deposited on 6 mm armor plates using an automated hardfacing device, and subsequently characterized with respect to their microstructure, phase composition, and ballistic performance. Thermodynamic calculations and microscopy revealed an austenitic matrix reinforced by hard boride inclusions. By increasing the Mo and B concentrations, the alloy solidification shifted from a primary austenite + austenite boride mixture to a primary boride + austenite boride mixture structure. The compositions with high Mo:B ratio yielded a ~25% volume fraction of $Mo_2(Fe,Mn)B_2$ borides. Ballistic tests using 7.62 mm steel-core bullets (~830 m/s) showed that uncoated Armox 440T was completely perforated, whereas all hardfaced plates prevented penetration. Notably, coatings with higher boride content eliminated rear-side spalling, indicating superior energy absorption and projectile fragmentation. These findings demonstrate that FCAW-applied hypereutectic Fe–Mo–Mn–B–C hardfacing alloys can significantly improve the ballistic performance of armor plates.

Key words: hardfacing, flux-cored arc welding, boride reinforcement, Armox 440T, ballistic resistance, austenitic manganese steel

INTRODUCTION

Enhancing the protection level of military equipment remains a challenging task, driven by the rapid evolution of weapons technology, which leads to growing threats. As munitions are increasingly designed for higher velocities, advanced ballistic materials, and refined impact mechanisms, armor systems must continuously adapt to meet these escalating demands [1, 2]. Modern research efforts encompass a broad spectrum of innovations in materials engineering, including alloys, ceramics, and composites. Functionally graded ceramic coatings help reduce localized deformation under impact, enhancing armor protection [3, 4]. Likewise, plasma electrolytic oxidation improves corrosion and wear resistance in multi-layer metals, ensuring long-term armor integrity [5]. Additionally, armor steels continue to be widely utilized for military vehicles and individual protection.

Simultaneously, manufacturing methods are evolving to incorporate high-productivity welding (hardfacing) processes and specialized heat treatments that optimize the balance between strength, toughness, and hardness in armor components. Restoration using flux-cored welding with high-manganese steel and carbide reinforcements effectively improves wear and impact resistance [6, 7, 8, 9], suggesting its potential for strengthening armor steel. Moreover, constraints related to cost, weight, and practicality in military applications necessitate approaches that balance performance with logistical feasibility.

These challenges aim to deliver robust solutions capable of withstanding ballistic and blast impacts while also extending service life, reducing downtime, and maintaining mobility in demanding operational environments. By integrating cutting-edge materials supported by computational modeling and modern surface engineering technologies, new Fe-based armor materials emerge as promising candidates to achieve superior protection without compromising critical aspects such as maneuverability, cost-effectiveness, and ease of manufacturing.

LITERATURE REVIEW

Although ceramic materials particularly those based on oxides [10], carbides, or advanced composites [11, 12] have found wide application in modern armor systems, steels and metallic alloys remain essential due to their comparatively low cost and ease of fabrication. While ceramics often exhibit exceptional hardness and ballistic performance, their manufacturing can be more complex and expensive. In contrast, steel-based solutions provide a balance of affordability, strength, and toughness that continues to make them a practical choice for a broad range of military and civilian protective applications. For the improving of the ballistic resistance, a combination of high-chromium alloy and austenitic steel was applied to low-alloy medium-carbon steel grade S355JR [13]. According to in [14], the aluminum alloy AlMgSi07.F25 has proven to be an unsuitable material. However, it can be used for surface treatment of ferrous components. The results demonstrated that the highest achieved ballistic resistance corresponded to Level III according to the NIJ standard. Alternatively, authors in [15] applied the laser cladding method to armor steel Armox 500T using Metco 42C powders, forming a martensitic stainless-steel structure with a hardness of approximately 620 HV. However, due to the limited thickness of the deposited layer (up to 1 mm), the method did not effectively increase ballistic resistance despite the high-quality fusion zone and absence of deformations.

Recently, researchers have focused significantly on enhancing the ballistic resistance of joints connecting armor plates in military vehicles. The complexity of this task lies in maintaining a balance between ballistic resistance, which involves the presence of hard phases, and weldability of alloys with armor steels. To address this issue, authors in [16] joined armor plates made of ARMOX 500T steel (Class 2 protection according to NATO standards) using a combination of chromium-nickel stainless steel electrodes Lincoln Electric MIG 309L Si (underlayer) and wear-resistant alloy Durmat FD 739, an Fe–Mo–W–Nb–Cr–B alloying system (top layer). Results indicated that only multi-layer cladding with wear-resistant material in the joint zone provided ballistic resistance higher than that of armor plates. However, fractures had a brittle character and occurred both in fusion zones and within the weld body. Similar approaches have been explored in structural applications where integrity is critical, such as the behaviour of closable cracks in thin shells under bending loads [17, 18, 19, 20, 21, 22]. Understanding structural response under dynamic conditions remains key to optimizing armor performance. In addition, recent research on frictional damping elements in protective systems shows that integrating armor plates with specialized damping structures can further improve impact resistance [23, 24, 25]. By using damping elements, stress concentrations [26] can be reduced and some of the impact energy can be absorbed, potentially reducing the risks of localized failures in armor plate applications.

Nevertheless, chromium-nickel austenitic steels are most widely used for joining armor plates [27, 28, 29], providing welded joints with high impact toughness despite significantly lower ballistic resistance compared to armor steels. Enhancing the ballistic resistance of such steels to the level of armor plates is achievable by expanding the alloying system to form specific hard reinforcement phases. Such phases include ternary borides of the types $M^{I}_{2}M^{II}B_2$ (space group P4/mbm) and $M^{I}M^{II}_{2}B_4$ (space group Immm), where M_I = Fe, Ni, Cr and M^{II} = Nb, Mo, W, Cr. Previous studies [30, 31] demonstrated that the ternary boride Mo_2FeB_2 readily forms via the FCAW method during deposition onto carbon steels. Similar behavior is expected when expanding the alloying system of chromium-nickel austenitic steels from Fe–Cr–Ni to Fe–Cr–Ni–Mo–B. This can lead to the formation of various hard phases, such as solid solutions $Mo_2(Fe,Cr,Ni)B_2$ and $Mo(Fe,Cr,Ni)B_4$, characterized by increased microhardness and ductility. Notably, due to the flexibility of FCAW technology, it is possible to obtain different phases and their varying concentrations in welded (cladded) joints [32, 33]. This allows ballistic resistance in the armor plate joint area to approach the level characteristic of the armor plates themselves. It is worth noting that FCAW technique presents several key advantages for the hardfacing and joining of armor plates. Firstly, FCAW delivers a high deposition rate, significantly surpassing traditional welding methods, which allows rapid build-up of thick, wear-resistant layers. Additionally, FCAW offers considerable flexibility in alloy selection, enabling the integration of specialized hard phases such as ternary borides (e.g., Mo_2FeB_2 or or $Mo_2(Fe,Mn,Cr,Ni)B_2$ solid solutions). The FCAW method also allows precise control over the type, distribution, and concentration of these reinforcement phases, thus optimizing both hardness and ductility based on operational demands. Moreover, FCAW ensures high-quality welds characterized by excellent fusion, minimal defects, and reduced deformation risks. The robustness and portability of FCAW equipment further support its application in challenging field conditions, facilitating timely repairs and reinforcements directly at the site of military operations. Lastly, FCAW is cost-effective, combining relatively low equipment and operational costs with efficient material usage and enhanced productivity. These collective advantages highlight FCAW as a versatile, reliable, and economically beneficial welding method, ideally suited for demanding military armor applications.

Mathematical approaches for numerical simulation of ballistic analysis for high-performance armor and composite materials are developed in [34, 35]. The obtained results can be improved and deepened by using more powerful analytical methods from [36, 37, 38].

The objective of this study was to evaluate the effectiveness of the flux-cored arc welding (FCAW) method in enhancing the ballistic resistance of steel armor plates through the application of electrode materials based on the Fe–Mo–Mn–B–C alloy system. These alloys promote the formation of an austenitic surface layer reinforced by boride strengthening phases. Such phase composition allows to combine deformation strengening by TWIP or TRIP mehanizms and dispersion hardeninig. To achieve this objective, the following tasks were undertaken:

- investigate the microstructure and phase composition of Fe–Mo–Mn–B–C hardfacing alloys with varying Mo and B contents;
- conduct ballistic testing of the hardfaced armor plates.

MATERIALS AND METHODS

The raw materials used for the production of flux-cored electrode wires included molybdenum powder of grade PM manufactured by GrandLada Co., Ltd (Ukraine) with particle sizes ranging from 1 to 10 μm (Fig. 1a), boron carbide (B_4C) of F120 fraction (Fig. 1b) manufactured by PJSC "ZAPOROZHABRAZIV" (Ukraine), and ferromanganese powder of grade FM95 produced by PJSC "Nikopol Ferroalloy Plant" (Ukraine).

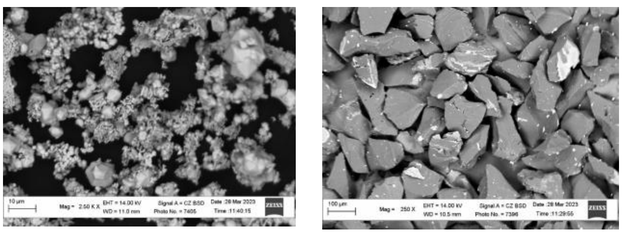

a b

Fig. 1 Morphology of the initial powder particles: Mo (a) and B_4C (b)

For hardfacing, specialized consumables were fabricated in the form of a flux-cored wire, specifically designed with a single-lock construction [31]. The outer sheath, providing structural integrity and electrical conductivity during deposition, was composed of 08kp grade low-carbon steel. This consumable possessed nominal cross-sectional dimensions of 8×2.5 mm. This specific geometry and construction method enabled the achievement of a significant powder fill coefficient, calculated at 40%. Such a high fill factor is crucial as it ensures that a substantial volume fraction of the core, containing the requisite alloying elements, is delivered to the weld pool. This facilitates the formation of a weld overlay deposit with the desired metallurgical composition and consequently, the necessary performance characteristics.

The calculated compositions of the deposited layers produced using the developed electrodes are listed in Table 1.

Table 1
Composition of the experimental hardfacing alloys

Sample	Composition, wt. %				
	Mn	Mo	B	C	Fe
C1	16.5	7.0	1.0	0.9	the rest
C2	16.1	9.6	1.1	0.9	the rest
C3	15.7	11.7	1.3	0.9	the rest
C4	15.0	15.0	1.7	0.8	the rest

Computational thermodynamic modeling, grounded in the CALPHAD methodology, was employed to predict the stable phases and their equilibrium proportions within the designed hardfacing alloys. These simulations were performed using the Thermo-Calc 2023 software package, incorporating requisite thermodynamic data either directly sourced from or validated against experimental and theoretical findings reported in [39, 40, 41, 42]. Understanding the predicted phase composition is fundamental for rationalizing the expected microstructure and performance characteristics of the hardfaced layers.

The samples for investigation were produced by automated hardfacing onto Armox 440T steel substrates using a laboratory FCAW system mounted on a three-axis universal table (Fig. 2). The deposition process was carried out under constant current conditions of 150-180 A with reverse polarity and an arc voltage of 18-22 V.

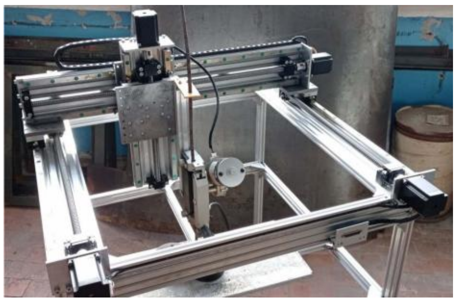

Fig. 2 Laboratory automated FCAW machine

Microstructural characterization of the hardfaced layers and morphological assessment of the worn surfaces were conducted using scanning electron microscopy (SEM) operating in the backscattered electron (BSE) mode. A ZEISS EVO 40XVP SEM, located at the Center for Collective Use of Scientific Instruments "Center for Electron Microscopy and X-ray Microanalysis" of the Karpenko Physico-Mechanical Institute of the National Academy of Sciences of Ukraine (Lviv, Ukraine), was employed for these investigations. The elemental chemical composition of the constituent phases was determined using energy-dispersive X-ray spectroscopy (EDS) coupled to the SEM. Acknowledging the inherent limitations of EDS in accurately quantifying light elements like boron, the stoichiometry of the observed boride phases was primarily inferred from the measured ratios of the metallic constituents.

Ballistic resistance evaluation was performed on 6 mm nominal thickness armor plates composed of Armox® 440T steel. The testing methodology adhered to the Ukrainian national standard DSTU 8782:2018, corresponding to protection Class 4 under this standard. Trials involved utilizing a Dragunov SVD rifle firing 7.62×54 mm LPS (Light Pistol Bullet with Steel core) ammunition, characterized by a non-hardened mild steel core. Tests were conducted at a controlled standoff distance of 10 meters, ensuring projectile impact velocities were maintained within the specified range of 830±15 m/s. For comparison with NATO standards, this impact velocity is closely aligned with the requirements specified for NATO STANAG 4569 Level 1.

After the ballistic tests, the hardness of the damaged regions was measured using a portable hardness tester (NOVOTEST T-UD2) on the Vickers scale. The resulting hardness was calculated as the average value of five measurements.

RESULTS AND DISCUSSION

Pseudobinary section of the Fe–Mn–Mo–B–C system along the line $Fe_{0.775}Mn_{0.18}C_{0.045}$–MoB (Fig. 3) corresponds to the mixed peritectic and eutectic-like type.

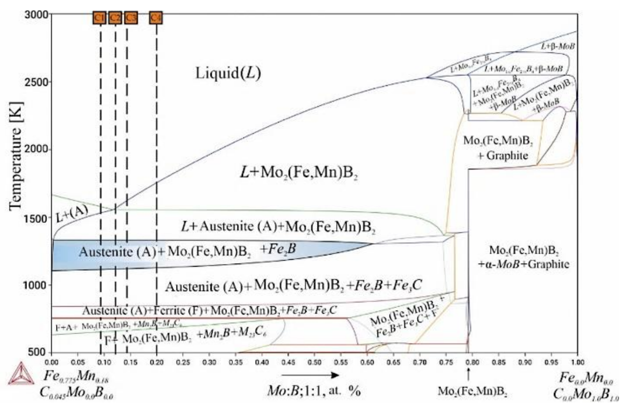

***Fig. 3** Pseudobinary section of the Fe–Mn–Mo–B–C system along the $Fe_{0.775}Mn_{0.18}C_{0.045}$–MoB line*

The lowest melting point is approximately 1560 K, and the alloy consists of ~15 vol.% $Mo_2(Fe,Mn)B_2$ (with the remainder being austenite), forming over a relatively wide temperature range of ~230 K. In the low-temperature region, within the concentration range relevant for designing hardfacing materials (up to 50 vol.% MoB), the stable phases besides austenite and $Mo_2(Fe,Mn)B_2$ – include Fe- and Mn-based borides of the M_2B type, Mn-alloyed cementite, the complex carbide $M_{23}C_6$, and ferrite. The phase evolution of the alloy C1 (Fig. 4) begins with the crystallization of austenite within the temperature range of 1590-1530 K, followed by a transformation of the remaining liquid according to the reaction: L→Austenite+$Mo_2(Fe,Mn)B_2$. At the solidus point of this alloy (~1340 K), a minor amount (up to ~1 vol.%) of Fe_2B phase forms. This is attributed to a slight deviation of the $Mo_2(Fe,Mn)B_2$ phase from stoichiometry, specifically a reduction in boron content. As the temperature decreases further, the cementite phase becomes stabilized at approximately 1100 K, with its volume fraction increasing up to 18 vol.% by ~760 K. At this temperature, according to the phase diagram, cementite undergoes decomposition with the formation of the complex carbide phase $(Fe,Mn)_{23}C_6$. It is worth noting that similar formation of cementite and subsequent solid-state transformations involving this phase are generally characteristic of Hadfield steel and other TWIP steels. However, this phenomenon is considered undesirable, as it leads to the depletion of manganese in the steel, thereby reducing its strain hardening capability. Strategies to prevent the formation of cementite include alloying or austenitization followed by rapid cooling, which is typical of the hardfacing process.

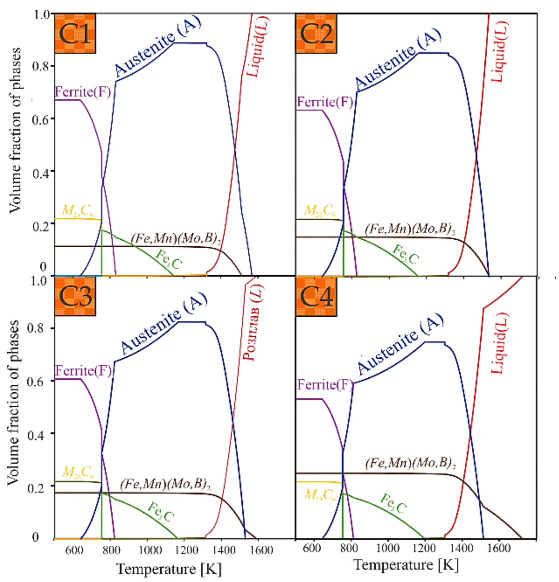

***Fig. 4** Calculated temperature-dependent phase compositions (volume fractions) for alloys C1–C4 based on the Fe–Mn–Mo–B–C system*

The microstructure of alloy C1 (Fig. 4) corresponds to the intermediate temperature range (1120–1320 K) of the calculated section (Fig. 4) and consists of two structural components: austenite, which forms from the melt as dendritic crystals exceeding 50 µm in length (the predominant constituent), and rod-like mixture of austenite + $Mo_2(Fe,Mn)B_2$. The latter is evidently formed via a mechanism similar to that of ledeburite in steels and can be conventionally described as a matrix of $Mo_2(Fe,Mn)B_2$ phase penetrated by austenitic "fibers". The crystallization of alloy C2 (Fig. 4) begins at the temperature and proceeds similarly to alloy C1.

Its microstructure is represented by mixture of austenite and the $Mo_2(Fe,Mn)B_2$ (Fig. 5). For the alloys C3 and C4 crystallization begins with the formation of primary $Mo_2(Fe,Mn)B_2$ phase crystals in the high-temperature region (above 1500 K) of the calculated polythermal section (Fig. 5).

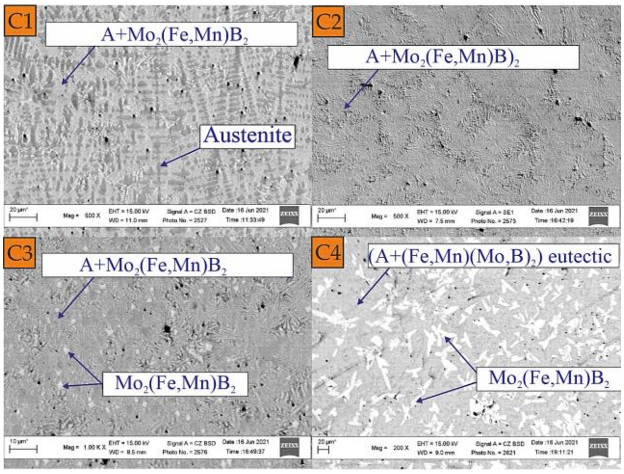

Fig. 5 Microstructure of alloys with varying contents of equimolar amounts of Mo and B according to the polythermal section

A comparative analysis of the microstructures of these alloys (Fig. 5) shows that the main difference between alloys C3 and C4 lies in the size of the primary $Mo_2(Fe,Mn)B_2$ phase particles. Specifically, in alloy C4, the majority of boride phase particles are in the range of 20-40 µm, which is nearly an order of magnitude larger than in alloy C3. This significant size difference is attributed to the higher crystallization onset temperature of alloy C4 (1755 K) compared to that of alloy C3 (1620 K), resulting in a broader primary crystallization interval for the $Mo_2(Fe,Mn)B_2$ phase.

The transition from the alloy C1 to the alloy C4 is accompanied by a proportional increase in the volume fraction of the $Mo_2(Fe,Mn)B_2$ phase from 10% to 25%, along with a corresponding decrease in the amount of austenite within the two-phase regions: austenite + $Mo_2(Fe,Mn)B_2$.

Evaluation of the ballistic performance of the untreated 6 mm Armox® 440T steel plate (as-delivered, non-hardfaced) demonstrated insufficient resistance against the defined threat. Complete perforation of the armor specimen occurred during the test. As depicted in Figure 6, this failure was characterized by substantial plastic deformation, including noticeable bulging and material extrusion, concentrated on the exit face of the plate.

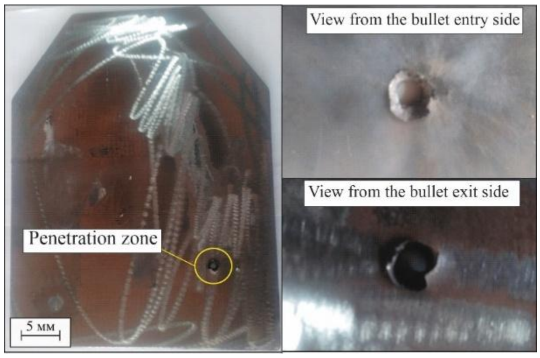

Fig. 6 Ballistic test results for an armor plate manufactured from Armox® 440T steel

To enhance the ballistic resistance of Armox® 440T armor plates, a single-layer hardfacing approximately 3 mm thick was applied using the developed electrode materials. For comparative analysis, alloys C1-C4 were deposited on different sections of the strike face of the armor plate (Fig. 7a). Ballistic test results (Fig. 7b) indicate that no complete penetration occurred in any of the tested materials. However, in the regions corresponding to layers hardfaced with C1 and C2 alloys, localized damage in the form of partial spalling was observed on the rear surface. In contrast, the zones hardfaced with C3 and C4 showed no visible signs of deformation or failure on the plate's rear side.

Meanwhile, the areas on the strike face protected by C3 and C4 exhibited a combination of plastic and brittle failure, as well as surface-layer delamination. This damage mode arises from the combined resistance to ballistic impact provided by the austenitic matrix – undergoing twinning-induced plasticity and the ceramic reinforcing phase, whose high hardness (~24 GPa) results from strong covalent bonds (B–B, Mo–B, and Fe(Mn)–B).

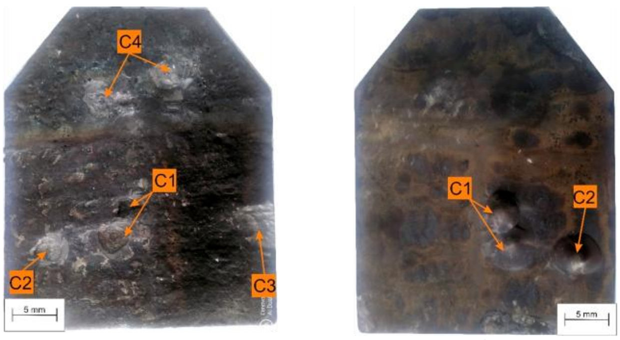

a b

Fig. 7 Ballistic test results for hardfaced Armox® 440T steel armor plates: (a) the strike face and (b) the rear side after impact

The hardness measurement procedure is illustrated in Fig. 8, and the corresponding results are listed in Table 2.

***Fig. 8** The harndness measurement procedure test results for hardfaced Armox® 440T steel armor plates after ballistic tests*

Table 2
Hardness test results for hardfacing layers with different compositions

Sample	Hv, GPa	
	Before tests	After tests
C1	5.32	5.82
C2	5.64	6.01
C3	5.95	6.17
C4	6.36	6.40

Analysis of the hardness measurements reveals that while an increase in the Mo:B content leads to higher initial hardness, the degree of work hardening after ballistic testing shows a decreasing trend. This phenomenon is attributed to the mechanical constraint of the austenite matrix within the rigid boride framework (as observed in samples C3 and C4, Fig. 5), which limits its capacity for intensive deformation strengthening. Therefore, the deformation strengthening capability of austenite alone is insufficient to provide effective protection for Armox® 440T against high-energy ballistic impacts. The obtained results demonstrate good agreement with data presented in [16], where the hardness varies from 1.9 to 8.61 GPa depending on the number of welding (hardfacing) passes.

CONCLUSIONS

FCAW-deposited Fe–Mo–Mn–B–C hardfacings with increasing Mo and B contents result in an austenitic matrix reinforced by up to ~25 vol.% $Mo_2(Fe,Mn)B_2$ borides. This higher boride content significantly raises surface hardness (borides ~20-25 GPa) while retaining sufficient austenite to absorb impact energy through twinning-induced plasticity. Ballistic tests show that 6 mm Armox® 440T is fully perforated by a 7.62 mm projectile at ~830 m/s, but a 3 mm hardfaced layer prevents penetration in all alloys. Compositions with Mo:B content up to 12 at.% exhibit minor back-face spalling, whereas coatings with Mo:B below 12 at.% (C3 and C4) display no visible damage on the rear side, indicating superior ballistic protection and energy absorption. Despite the relatively large boride particles (~20-40 µm) in the most highly alloyed sample (C4), no detrimental cracking occurs, and ballistic performance is maximized. Consequently, hypereutectic Fe–Mo–Mn–B–C alloys are the most effective for FCAW-based hardfacing, offering a versatile solution to upgrade armor plates against modern ballistic threats.

ACKNOWLEDGEMENTS

The authors express their sincere gratitude and respect to the Armed Forces of Ukraine, who made it possible to complete the preparation of this article for publication. The authors also express their gratitude to the Ministry of Science and Education of Ukraine for grants for the implementation of projects 0123U101858 and 0124U000473.

REFERENCES

[1] A. Malik, F. Nazeer, and Y. Wang, "A prospective way to achieve ballistic impact resistance of lightweight magnesium alloys," *Metals (Basel)*, vol. 12, no. 2, pp. 1-3, 2022, doi: 10.3390/met12020241.

[2] E.Ch. Tsirogiannis, E. Daskalakis, M.H. Hassan, A.M. Omar, and P. Bartolo, "Ballistic design and testing of a composite armour reinforced by CNTs suitable for armoured vehicles," *Defence Technology*, vol. 32, pp. 173-195, 2024, doi: 10.1016/j.dt.2023.04.013.

[3] Y. Wang et al., "Ballistic performance of functionally graded B4C/Al composites without abrupt interfaces: Experiments and simulations," *Journal of Materials Research and Technology*, vol. 25, pp. 1011-1029, 2023, doi: 10.1016/j.jmrt.2023.06.021.

[4] I. Shatskyi, M. Makoviichuk, L. Ropyak, and A. Velychkovych, "Analytical model of deformation of a functionally graded ceramic coating under local load," *Ceramics*, vol. 6, no. 3, pp. 1879-1893, 2023, doi: 10.3390/ceramics6030115.

[5] L. Ropyak, T. Shihab, A. Velychkovych, O. Dubei, T. Tutko, and V. Bilinskyi, "Design of a two-layer Al–Al2O3 coating with an oxide layer formed by the plasma electrolytic oxidation of Al for the corrosion and wear protections of steel," *Progress in Physics of Metals*, vol. 24, no. 2, pp. 319-365, 2023.

[6] L. Ropyak, T. Shihab, A. Velychkovych, O. Dubei, T. Tutko, and V. Bilinskyi, "Design of a two-layer Al–Al2O3 coating with an oxide layer formed by the plasma electrolytic oxidation of Al for the corrosion and wear protections of steel," *Progress in Physics of Metals*, vol. 24, no. 2, pp. 319-365, 2023.

[7] V. Lozynskyi et al., "Prediction of phase composition and mechanical properties Fe–Cr–C–B–Ti–Cu hardfacing alloys: Modeling and experimental validations," *Heliyon*, vol. 10, no. 3, p. e25199, 2024, doi: 10.1016/j.heliyon.2024.e25199.

[8] P. Prysyazhnyuk, M. Molenda, T. Romanyshyn, L. Ropyak, L. Romanyshyn, and V. Vytvytskyi, "Development of a hardbanding material for drill pipes based on high-manganese steel reinforced with complex carbides," *Acta Montanistica Slovaca*, vol. 27, no. 3, pp. 1-10, 2022.

[9] P. Prysyazhnyuk, O. Ivanov, O. Matvienkiv, S. Marynenko, O. Korol, and I. Koval, "Impact and abrasion wear resistance of the hardfacings based on high-manganese steel reinforced with multicomponent carbides of Ti–Nb–Mo–VC system," *Procedia Structural Integrity*, vol. 36, pp. 130-136, 2022, doi: 10.1016/j.prostr.2022.01.014.

[10] V. Kulyk et al., "The effect of sintering temperature on the phase composition, microstructure, and mechanical properties of yttria-stabilized zirconia," *Materials (Basel)*, vol. 15, no. 8, p. 2707, 2022, doi: 10.3390/ma15082707.

[11] I. Solodkyi et al., “Hierarchical composites of B4C–TiB2 eutectic particles reinforced with Ti,” *Ceramics International*, vol. 46, no. 18, pp. 28132-28144, 2020, doi: 10.1016/j.ceramint.2020.07.312.

[12] M. Ayvaz and H. Cetinel, “Ballistic performance of powder metal Al5Cu–B4C composite as monolithic and laminated armor,” *Materials Testing*, vol. 63, no. 6, pp. 512-518, 2021, doi: 10.1515/mt-2020-0084.

[13] M. Sözeri, U. Özdemir, T. Fındık, and H. Karakoç, “Comparative study of hardfacing applications on structural steel surfaces to improve ballistic properties,” *Materials Today Communications*, vol. 38, p. 107733, 2024, doi: 10.1016/j.mtcomm.2023.107733.

[14] P. Kopas, M. Blatnicky, M. Sága and M.Vasko, “Identification of mechanical properties of weld joints of AlMgSi07.F25 aluminium alloy”. *Metalurgija*, Vol. 56, Issue 1-2, pp. 99-102. Published 2017.

[15] E. Altuncu and M. Tarım, “Laser cladding of martensitic stainless steels on armor steels,” *Emerging Materials Research*, vol. 9, no. 1, pp. 1-4, 2020, doi: 10.1680/jemmr.18.00120.

[16] I. Garašić, M. Jurica, A. Barišić, and D. Iljkić, “Determination of ballistic properties on ARMOX 500T steel welded joint,” *Engineering Review*, vol. 39, no. 2, pp. 186-196, 2019, doi: 10.30765/er.39.2.8.

[17] I.P. Shats’kyi, “Closure of a longitudinal crack in a shallow cylindrical shell in bending,” *Materials Science*, vol. 41, no. 2, pp. 186-191, 2005, doi: 10.1007/s11003-005-0149-z.

[18] I.P. Shats’kyi and M.V. Makoviichuk, “Contact interaction of crack lips in shallow shells in bending with tension,” *Materials Science*, vol. 41, no. 4, pp. 486-494, 2005, doi: 10.1007/s11003-006-0006-8.

[19] K.M. Dovbnya and N.A. Shevtsova, “Studies on the stress state of an orthotropic shell of arbitrary curvature with the through crack under bending loading,” *Strength of Materials*, vol. 46, no. 3, pp. 345-349, 2014, doi: 10.1007/s11223-014-9556-4.

[20] I.P. Shats’kyi and M.V. Makoviichuk, “Analysis of the limiting state of cylindrical shells with cracks with regard for the contact of crack lips,” *Strength of Materials*, vol. 41, no. 5, pp. 560-564, 2009, doi: 10.1007/s11223-009-9166-8.

[21] I.P. Shatskii and N.V. Makoviichuk, “Effect of closure of collinear cracks on the stress–strain state and the limiting equilibrium of bent shallow shells,” *Journal of Applied Mechanics and Technical Physics*, vol. 52, no. 3, pp. 464-470, 2011, doi: 10.1134/s0021894411030175.

[22] M.V. Makovijchuk, T.M. Daliak, and I.P. Shatskij, “Interaction of contact crack with collinear slit under shallow spherical shell bending,” *International Applied Mechanics*, vol. 60, no. 2, pp. 171-178, 2024, doi: 10.1007/s10778-024-01271-z.

[23] I.A. Shah et al., “Finite element analysis of the ballistic impact on auxetic sandwich composite human body armor,” *Materials (Basel)*, vol. 15, no. 6, p. 2064, 2022, doi: 10.3390/ma15062064.

[24] I. Shatskyi and A. Velychkovych, “Analytical model of structural damping in friction module of shell shock absorber connected to spring,” *Shock and Vibration*, pp. 1-17, 2023, doi: 10.1155/2023/4140583.

[25] A. Velychkovych, V. Mykhailiuk, and A. Andrusyak, “Numerical model for studying the properties of a new friction damper developed based on the shell with a helical cut,” *Applied Mechanics*, vol. 6, no. 1, p. 1, 2025, doi: 10.3390/applmech6010001.

[26] M. Handrik, P. Kopas, V. Baniari, M. Vasko and M. Saga, “Analysis of stress and strain of fatigue specimens localised in the cross-sectional area of the gauge section testing on bi-axial fatigue machine loaded in the high-cycle fatigue region,“ *XXI Polish-Slovak scientific conference machine modeling and simulations* MMS 2016, Vol. 177, pp. 516-519, DOI10.1016/j.proeng.2017.02.254

[27] E.R.S. Souza, R.P. Weber, S.N. Monteiro, and S. de S. Oliveira, “Microstructure effect of heat input on ballistic performance of welded high strength armor steel,” *Materials (Basel)*, vol. 14, no. 19, p. 5789, 2021, doi: 10.3390/ma14195789.

[28] T. Özdemir, “Mechanical & microstructural analysis of armor steel welded joints,” *Uluslararası Muhendislik Arastirma ve Gelistirme Dergisi*, pp. 166-175, 2020, doi: 10.29137/umagd.488104.

[29] S.N. Kumar, V. Balasubramanian, S. Malarvizhi, A.H. Rahman, and V. Balaguru, “Effect of welding consumables on shielded metal arc welded ultra high hard armour steel joints,” *Journal of the Mechanical Behavior of Materials*, vol. 31, no. 1, pp. 8-21, 2022, doi: 10.1515/jmbm-2022-0002.

[30] O. Ivanov, P. Prysyazhnyuk, D. Lutsak, O. Matviienkiv, and V. Aulin, “Improvement of abrasion resistance of production equipment wear parts by hardfacing with flux-cored wires containing boron carbide/metal powder reaction mixtures,” *Management Systems in Production Engineering*, vol. 28, no. 3, pp. 178-183, 2020, doi: 10.2478/mspe-2020-0026.

[31] M. Bembenek, P. Prysyazhnyuk, T. Shihab, R. Machnik, O. Ivanov, and L. Ropyak, “Microstructure and wear characterization of the Fe-Mo-B-C-based hardfacing alloys deposited by flux-cored arc welding,” *Materials (Basel)*, vol. 15, no. 14, 2022, doi: 10.3390/ma15145074.

[32] M. Student, A. Vojtovych, H. Pokhmurska, O. Maruschak, O. Student, and P. Maruschak, “Mechanical characteristics and wear resistance of the cladding layers obtained by melting of cored wires with simultaneous vibration of substrate,” *Strojnícky časopis – Journal of Mechanical Engineering*, vol. 69, no. 1, pp. 109-122, 2019, doi: 10.2478/scjme-2019-0009.

[33] S.T.A. Shihab, P. Prysyazhnyuk, R. Andrusyshyn, L. Lutsak, O. Ivanov, and I. Tsap, “Forming the structure and the properties of electric arc coatings based on high manganese steel alloyed with titanium and niobium carbides,” *Eastern-European Journal of Enterprise Technologies*, vol. 1, no. 12 (103), pp. 38-44, 2020, doi: 10.15587/1729-4061.2020.194164.

[34] D. Li et al., “Ballistic analysis of high-performance armor steel by numerical simulation,” *Scientific Reports*, vol. 14, no. 1, 2024, doi: 10.1038/s41598-024-62482-5.

[35] D. Ma, R. Scazzosi, and A. Manes, “Modeling approaches for ballistic simulations of composite materials: Analytical model vs. finite element method,” *Composites Science and Technology*, vol. 248, p. 110461, 2024, doi: 10.1016/j.compscitech.2024.110461.

[36] Y. Striletskyi, L. Ropyak, and A. Bandura, “Method of oscillation excitation for investigation of inconsistency of coating deposition on long parts,” *Vibroengineering Procedia*, vol. 57, pp. 25-31, 2024, doi: 10.21595/vp.2024.24567.

[37] A. Bandura and O. Skaskiv, “Functions analytic in a unit ball of bounded L-index in joint variables,” *Journal of Mathematical Sciences*, vol. 227, no. 1, pp. 1-12, 2017, doi: 10.1007/s10958-017-3570-6.

[38] A. Bandura and O. Skaskiv, "Entire functions of bounded L-index: Its zeros and behavior of partial logarithmic derivatives," *Journal of Complex Analysis*, pp. 1-10, 2017, doi: 10.1155/2017/3253095.

[39] P. Prysyazhnyuk and D. Di Tommaso, "The thermodynamic and mechanical properties of Earth-abundant metal ternary boride Mo2(Fe,Mn)B2 solid solutions for impact- and wear-resistant alloys," *Materials Advances*, vol. 4, no. 17, pp. 3822-3838, 2023, doi: 10.1039/d3ma00313b.

[40] B. Hallstedt, A.V. Khvan, B.B. Lindahl, M. Selleby, and S. Liu, "PrecHiMn-4–a thermodynamic database for high-Mn steels," *Calphad*, vol. 56, pp. 49–57, 2017, doi: 10.1016/j.calphad.2016.11.006.

[41] V.A. Tatarenko and T.M. Radchenko, "The application of radiation diffuse scattering to the calculation of phase diagrams of F.C.C. substitutional alloys," *Intermetallics*, vol. 11, no. 11-12, pp. 1319-1326, 2003, doi: 10.1016/s0966-9795(03)00174-2.

[42] S.M. Bokoch and V.A. Tatarenko, "A semi-empirical parameterization of interatomic interactions based on the statistical-thermodynamic analysis of the data on radiation diffraction and phase equilibria in F.C.C.–Ni–Fe alloys," *Solid State Phenomena*, vol. 138, pp. 303-318, 2008, doi: 10.4028/www.scientific.net/ssp.138.303.

Pavlo Prysyazhnyuk
ORCID ID: 0000-0002-8325-3745
Ivano-Frankivsk National Technical University
of Oil and Gas
Institute of Engineering Mechanics and Robotics
Department of Computerized Mechanical Engineering
Karpatska 15, 076019 Ivano-Frankivsk, Ukraine
e-mail: pavlo1752010@gmail.com

Witold Biały
ORCID ID: 0000-0003-2313-0230
KOMAG Institute of Mining Technology
Pszczyńska 37, 44-101 Gliwice, Poland
e-mail: wbialy@komag.eu

Michał Bembenek (corresponding author)
ORCID ID: 0000-0002-7665-8058
AGH University of Krakow
Faculty of Mechanical Engineering and Robotics
Department of Manufacturing Systems
Adama Mickiewicza Ave. 30, 30-059 Kraków, Poland
e-mail: bembenek@agh.edu.pl

Vitalii Panchuk
ORCID ID: 0000-0002-2246-280X
Ivano-Frankivsk National Technical University
of Oil and Gas
Institute of Engineering Mechanics and Robotics
Department of Computerized Mechanical Engineering
Karpatska 15, 076019 Ivano-Frankivsk, Ukraine
e-mail: vitalii.panchuk@nung.edu.ua

Iuliia Medvid
ORCID ID: 0000-0001-7613-9189
Ivano-Frankivsk National Technical University
of Oil and Gas
Institute of Engineering Mechanics and Robotics
Department of Computerized Mechanical Engineering
Karpatska 15, 076019 Ivano-Frankivsk, Ukraine
e-mail: yuliia.medvid@nung.edu.ua

Zoia Duriagina
ORCID ID: 0000-0002-2585-3849
Lviv Polytechnic National University,
Departament of Materials Science
and Materials Ingineering
Stepan Bandera Street 12, 79013 Lviv, Ukraine
e-mail: zduriagina@gmail.com

Taras Romanyshyn
ORCID ID: 0000-0002-0856-1537
Ivano-Frankivsk National Technical University
of Oil and Gas
Institute of Information Technologies
Department of Software Engineering
Karpatska 15, 076019 Ivano-Frankivsk, Ukraine
e-mail: taras.romanyshyn@nung.edu.ua

Vasyl Vytvytskyi
ORCID ID: 0000-0003-3682-1612
Ivano-Frankivsk National Technical University
of Oil and Gas
Institute of Engineering Mechanics and Robotics
Department of Technical Mechanics, Engineering
and Computer Graphics
Karpatska 15, 076019 Ivano-Frankivsk, Ukraine
e-mail: vytvytskyi.v.s@gmail.com